Preprints (www.preprints.org) | NOT PEER-REVIEWED | Posted: 31 May 2020 doi:10.20944/preprints202005.0503.v1

Peer-reviewed version available at *Appl. Sci.* **2020**, *10*, 4337; doi:10.3390/app10124337

Article

A LOGARITHMIC TURBULENT HEAT TRANSFER MODEL IN APPLICATIONS WITH DIFFERENT LIQUID METALS

Roberto Da Vià [1,†,‡] and Sandro Manservisi [2,‡]

[1] CINECA, Italian university consortium, via Magnanelli 6/3, Bologna, 40033; r.davia@cineca.it
[2] University of Bologna, DIN, Montecuccolino Laboratory, Via dei colli 16, 40136 Bologna, Italy; sandro.manservisi@unibo.it

Featured Application: Authors are encouraged to provide a concise description of the specific application or a potential application of the work. This section is not mandatory.

Abstract: The study of turbulent heat transfer in liquid metal flows has gained interest because of applications in several industrial fields. The common assumption of similarity between the dynamical and thermal turbulence, namely the Reynolds analogy, has been proven to be not valid for these fluids. Many methods have been proposed in order to overcome the difficulties encountered in a proper definition of the turbulent heat flux, such as global or local correlations for the turbulent Prandtl number or four parameter turbulence models. In this work we assess a four parameter logarithmic turbulence model for liquid metals based on RANS approach. Several simulation results considering fluids with $Pr = 0.01$ and $Pr = 0.025$ are reported in order to show the validity of this approach. The Kays turbulence model is also assessed and compared with integral heat transfer correlations for a wide range of Peclet numbers.

Keywords: Turbulent heat transfer, Low-Prandtl fluids, RANS modeling, Logarithmic turbulence model

1. Introduction

The fluid-dynamics of low Prandtl number liquid metals is currently studied because of an increasing interest in the application of these fluids in engineering problems. Advanced nuclear reactor designs cooled with liquid metals have been proposed in the Generation IV Forum and some liquid metal fast nuclear reactors have been built and operated [1]. Liquid metal fluid dynamics is also studied in other engineering fields as they are considered possible coolants for new solar power systems [2]. These fluids show a low dynamical viscosity with a high thermal conductivity, thus resulting in a low Prandtl number. Liquid metals currently considered for Generation IV nuclear reactors are sodium and Lead-Bismuth eutectic. Depending on the operational temperature of the reactor the coolant Prandtl number changes, in particular with increasing temperature the Prandtl number decreases. The Prandtl number of Lead-Bismuth eutectic is in the range of 0.03 to 0.01 while sodium has a lower Prandtl with values ranging from 0.01 to 0.005 [3]. Despite the increasing interest for these fluids reliable computational tools for the study of turbulent heat transfer in complex industrial applications with liquid metals are still lacking in commercial codes. The study of reliable and robust computational techniques to deal with this problem is still in the development phase [1,4–8].

Direct Numerical Simulation and Large Eddy Simulation are being used to investigate these physical phenomena but an accurate prediction of heat transfer in industrial applications like heat exchangers or nuclear reactor pools cannot rely on these techniques for limitations of the available

© 2020 by the author(s). Distributed under a Creative Commons CC BY license.

Preprints (www.preprints.org) | NOT PEER-REVIEWED | Posted: 31 May 2020 doi:10.20944/preprints202005.0503.v1

Peer-reviewed version available at Appl. Sci. 2020, 10, 4337; doi:10.3390/app10124337

computational resources [5,6,9–12]. On the other hand, numerical data obtained with these simulation techniques are of strong interest for the validation of turbulence models based on Reynolds Averaging Navier-Stokes approach because they can be used to finely tune the turbulence model in the low Reynolds number regime. RANS modeling has been successfully employed in several Computational Fluid Dynamics areas, such as aeronautical, automotive, nuclear and many other fields where the studied fluid flow is turbulent and DNS is not affordable. In this framework it is very common to assume similarity between the dynamical and thermal turbulent transfer and therefore to define a constant turbulent Prandtl number as the ratio between the eddy viscosity and eddy thermal diffusivity. For fluids with $Pr \sim 1$ the turbulent Prandtl number is set to $Pr_t = 0.85 - 0.9$ but for liquid metal flows this assumption is known to be not valid [4,5,7].

Several solutions have been proposed to deal with this problem. One possible method is to use a correlation that gives the value of the turbulent Prandtl number as a function of the global parameters of the flow, such as Reynolds or Peclet numbers. By doing so a constant Pr_t is assumed on the whole domain but its value changes with the case studied. Recently a correlation for the turbulent Prandtl number as a function of the Peclet number has been suggested in [4]. Another possible solution is to define a local turbulent Prandtl number as a function of some flow variables as the one proposed by Kays [13]. In the work [5] the authors study this and other local or global correlations and compare the results obtained in a few test cases. They conclude that Kays correlation is the most reliable one among existing local correlations for RANS computations.

The key point in many of these approaches is that the correlation has to be defined and validated for each geometry. In this work we use a different approach and define the turbulent heat diffusivity with specific time scales which are resolved by the introduction of the rate dissipation of temperature and velocity fluctuations. This type of models have been already studied by some authors for forced convection and buoyant flows and should be more reliable in complex geometrical configurations [7,8,14–19]. In particular, in [8,17–19], a four parameter turbulence model for liquid metal flows has been developed and validated in several geometries. To extend this work we present a logarithmic k-Ω-k_θ-Ω_θ formulation of the four parameter turbulence model to improve its numerical robustness and the implementation of the boundary conditions as explained in [20]. Moreover we present numerical results obtained with two low Prandtl numbers, namely $Pr = 0.01$ and 0.025, in order to show the possibility of studying different fluids with a operational temperature range. Finally we report the results obtained by using the dynamical two-equation turbulence model together with Kays correlation with different Peclet numbers and compare all the results with available experimental correlations for the Nusselt number.

2. Transport equations and turbulence model

The Reynolds Averaged Navier-Stokes equations for incompressible flows can be written as

$$\boldsymbol{\nabla} \cdot \mathbf{u} = 0\,, \tag{1}$$

$$\rho \frac{\partial \mathbf{u}}{\partial t} + \rho(\mathbf{u} \cdot \boldsymbol{\nabla})\mathbf{u} = -\boldsymbol{\nabla} P + \boldsymbol{\nabla} \cdot \left[\mu \left(\boldsymbol{\nabla}\mathbf{u} + \boldsymbol{\nabla}\mathbf{u}^T\right) - \rho\overline{\mathbf{u}'\mathbf{u}'}\right] + \rho\mathbf{g}\,, \tag{2}$$

$$\rho C_p \left(\frac{\partial T}{\partial t} + (\mathbf{u} \cdot \boldsymbol{\nabla})T\right) = \boldsymbol{\nabla} \cdot \left[\lambda \boldsymbol{\nabla} T - \rho C_p \overline{\mathbf{u}'T'}\right] + Q\,, \tag{3}$$

where $\mathbf{u}$ is the average fluid velocity, P the pressure, T is the average temperature and Q represents the volumetric heat source or sink. The fluctuating quantities are denoted by the upper-script $'$. The RANS equations are similar to the Navier-Stokes equations, except for the terms $-\rho\overline{\mathbf{u}'\mathbf{u}'}$ and $-\rho C_p \overline{\mathbf{u}'T'}$, where the operator $\overline{(\cdot)}$ means the time average. These terms depend on the values of fluctuating velocity $\mathbf{u}$ and temperature T' and are introduced in (2-3) as a result of the time average of the convective terms. We normally refer to these new terms as the *Reynolds stresses* $\boldsymbol{\tau}^R$ and the *turbulent heat flux* $\mathbf{q}^R$ [21,22]

$$\boldsymbol{\tau}^R = \rho\overline{\mathbf{u}'\mathbf{u}'} \qquad \mathbf{q}^R = \rho C_p \overline{\mathbf{u}'T'}\,. \tag{4}$$

Preprints (www.preprints.org) | NOT PEER-REVIEWED | Posted: 31 May 2020 doi:10.20944/preprints202005.0503.v1

Peer-reviewed version available at Appl. Sci. 2020, 10, 4337; doi:10.3390/app10124337

These terms can be either calculated by the solution of proper transport equations or modeled using known variables. The first option is very expensive in terms of computational cost because it would add 9 transport equations, which need to be modeled, to the system (1-3). The latter option is the most used in RANS modeling because it allows to obtain reliable results with a smaller computational cost. With this method the Reynolds stresses and the turbulent heat flux are calculated using the mean velocity $\mathbf{u}$, the mean temperature T and two new variables, the eddy viscosity ν_t and the eddy heat diffusivity α_t. They are thus calculated as

$$\boldsymbol{\tau}^R = -\rho\nu_t\left(\boldsymbol{\nabla}\mathbf{u}+\boldsymbol{\nabla}\mathbf{u}^T\right)+\rho\frac{2k}{3}\mathbf{I}\,, \tag{5}$$

$$\mathbf{q}^R = -\rho C_p\alpha_t\,\boldsymbol{\nabla}T\,, \tag{6}$$

where the eddy viscosity ν_t and the eddy heat diffusivity α_t must be properly defined in the turbulence model. In (5) k represents the turbulent kinetic energy which is defined as

$$k=\frac{1}{2}\overline{\mathbf{u}'^2}\,. \tag{7}$$

With these new variables the system (1-3) becomes

$$\boldsymbol{\nabla}\cdot\mathbf{u}=0\,, \tag{8}$$

$$\frac{\partial\mathbf{u}}{\partial t}+\mathbf{u}\cdot\boldsymbol{\nabla}\mathbf{u}=-\frac{1}{\rho}\boldsymbol{\nabla}P+\boldsymbol{\nabla}\cdot\left[(\nu+\nu_t)\left(\boldsymbol{\nabla}\mathbf{u}+\boldsymbol{\nabla}\mathbf{u}^T\right)\right]+\mathbf{g}\,, \tag{9}$$

$$\frac{\partial T}{\partial t}+\mathbf{u}\cdot\boldsymbol{\nabla}T=\boldsymbol{\nabla}\cdot\left[(\alpha+\alpha_t)\,\boldsymbol{\nabla}T\right]+\frac{Q}{\rho C_p}\,. \tag{10}$$

For fully developed flows with a null volumetric source Q and with a uniform and constant heat flux per unit area q applied on wall surfaces, the temperature grows linearly with the axial coordinate. It is then possible to split the mean temperature field T as the sum of various contributions:

$$T(x,y,z)=T_{w0}-\tilde{T}(x,y)+\frac{dT}{dz}(z-z_{in})\,, \tag{11}$$

where T_{w0} is the wall temperature at the axial position z_{in}. The derivative dT/dz is a constant and uniform value across the transverse section of the pipe, so the term $T_{w0}+dT/dz(z-z_{in})$ is equal to the wall temperature at the generic axial position z. The temperature field $\tilde{T}(x,y)$ represents the difference between this wall temperature and the temperature of the transverse cross section. The field $\tilde{T}(x,y)$ does not depend on the axial coordinate. The temperature gradient along the axial direction dT/dz can be calculated through an integration of (10) on the whole domain, obtaining

$$\boldsymbol{\nabla}T\cdot\hat{a}=\frac{4qf_h}{w_{mid}\rho C_pD_h}\,, \tag{12}$$

where $\hat{a}$ is the unit vector parallel to the axial direction, w_{mid} is the average axial velocity on the cross section of the domain, D_h is the hydraulic diameter and f_h is the ratio between the heated and the wet perimeter of the domain cross section. The energy balance equation (10) in $\tilde{T}$ becomes

$$\frac{\partial\tilde{T}}{\partial t}+\mathbf{u}\cdot\boldsymbol{\nabla}\tilde{T}=\boldsymbol{\nabla}\cdot\left[(\alpha+\alpha_t)\,\boldsymbol{\nabla}\tilde{T}\right]+\mathbf{u}\cdot\hat{\mathbf{a}}\frac{4qf_h}{w_{mid}\rho C_pD_h}\,, \tag{13}$$

where $\hat{\mathbf{a}}$ is the unit vector in the axial direction. The last term in (13) is a source which depends on the heat flux on the wall and on the fluid velocity and geometry. This change of variables allows us to impose a homogeneous Neumann boundary condition on the inlet and outlet surfaces for $\tilde{T}$ and to set a simple Dirichlet condition on the wall, $\tilde{T}=T_{w0}$.

Preprints (www.preprints.org) | NOT PEER-REVIEWED | Posted: 31 May 2020 doi:10.20944/preprints202005.0503.v1

Peer-reviewed version available at Appl. Sci. 2020, 10, 4337; doi:10.3390/app10124337

2.1. Turbulence model k-Ω-k_θ-Ω_θ

In this paper we propose a new four parameters logarithmic turbulence model, the k-Ω-k_θ-Ω_θ, hereinafter referred to as the KLW model. The model is obtained through a change of state variables in the k-ε-k_θ-ε_θ turbulence model [8,15,23,24]. We recall the definitions of the turbulence variables k-ε-k_θ-ε_θ. k is the turbulent kinetic energy and ε its rate of dissipation. They are defined as

$$k := \frac{1}{2}\overline{\mathbf{u}'^2}, \qquad \varepsilon := \nu\overline{\|\boldsymbol{\nabla}\mathbf{u}'\|^2}. \tag{14}$$

k_θ is the mean squared temperature fluctuations value and ε_θ is its dissipation rate. They are defined as

$$k_\theta := \frac{1}{2}\overline{T'^2}, \qquad \varepsilon_\theta := \alpha\overline{\|\boldsymbol{\nabla}T'\|^2}. \tag{15}$$

To compute the time scales of turbulence we decide to employ the logarithmic values of k and k_θ specific dissipation rate ω and ω_θ,

$$\Omega = \ln\left(\frac{\varepsilon}{C_\mu k}\right), \qquad \Omega_\theta = \ln\left(\frac{\varepsilon_\theta}{C_\mu k_\theta}\right), \tag{16}$$

where C_μ is a model constant.

The introduction of logarithmic variables brings important advantages to the turbulence model robustness, in particular the original variables $\omega = \varepsilon/C_\mu k$ and $\omega_\theta = \varepsilon_\theta/C_\mu k_\theta$ are always kept positive because they are calculated as the exponential values of the new logarithmic variables. Another important feature is the fact that logarithmic variables have profiles which are smoother than the ones of the natural variables so a less fine mesh should be needed near the wall [20]. By substituting the new definitions (16) in the k-ε formulation of the turbulence model we obtain [8,15,23,24]

$$\frac{\partial k}{\partial t} + \mathbf{u}\cdot\boldsymbol{\nabla}k = \boldsymbol{\nabla}\cdot\left[\left(\nu + \frac{\nu_t}{\sigma_k}\right)\boldsymbol{\nabla}k\right] + \mathcal{P}_k - C_\mu\, k\, e^{\Omega}, \tag{17}$$

$$\begin{aligned}\frac{\partial \Omega}{\partial t} + \mathbf{u}\cdot\boldsymbol{\nabla}\Omega &= \boldsymbol{\nabla}\cdot\left[\left(\nu + \frac{\nu_t}{\sigma_\varepsilon}\right)\boldsymbol{\nabla}\Omega\right] + \\ &+ \frac{2}{k}\left(\nu + \frac{\nu_t}{\sigma_\varepsilon}\right)\boldsymbol{\nabla}k\cdot\boldsymbol{\nabla}\Omega + \left(\nu + \frac{\nu_t}{\sigma_\varepsilon}\right)\boldsymbol{\nabla}\Omega\cdot\boldsymbol{\nabla}\Omega + \\ &+ \frac{c_{\varepsilon 1} - 1}{k}\mathcal{P}_k - C_\mu\left(c_{\varepsilon 2} f_\varepsilon - 1\right)e^{\Omega},\end{aligned} \tag{18}$$

$$\frac{\partial k_\theta}{\partial t} + \mathbf{u}\cdot\boldsymbol{\nabla}k_\theta = \boldsymbol{\nabla}\cdot\left[\left(\alpha + \frac{\alpha_t}{\sigma_\theta}\right)\boldsymbol{\nabla}k_\theta\right] + \mathcal{P}_{k\theta} - C_\mu\, k_\theta\, e^{\Omega_\theta}, \tag{19}$$

$$\begin{aligned}\frac{\partial \Omega_\theta}{\partial t} + \mathbf{u}\cdot\boldsymbol{\nabla}\Omega_\theta &= \boldsymbol{\nabla}\cdot\left[\left(\alpha + \frac{\alpha_t}{\sigma_{\varepsilon_\theta}}\right)\boldsymbol{\nabla}\Omega_\theta\right] + \\ &+ \frac{2}{k_\theta}\left(\alpha + \frac{\alpha_t}{\sigma_{\varepsilon_\theta}}\right)\boldsymbol{\nabla}k_\theta\cdot\boldsymbol{\nabla}\Omega_\theta + \left(\alpha + \frac{\alpha_t}{\sigma_{\varepsilon_\theta}}\right)\boldsymbol{\nabla}\Omega_\theta\cdot\boldsymbol{\nabla}\Omega_\theta + \\ &+ \frac{c_{p1} - 1}{k_\theta}\mathcal{P}_{k\theta} + \frac{c_{p2}}{k}\mathcal{P}_k - \left(c_{d1} - 1\right)e^{\Omega_\theta} - c_{d2}C_\mu e^{\Omega}.\end{aligned} \tag{20}$$

The term $\mathcal{P}_k$ is the source term for the turbulent kinetic energy

$$\mathcal{P}_k := -\overline{u_i' u_j'}\frac{\partial u_i}{\partial x_j} = \frac{\nu_t}{2}\|\boldsymbol{\nabla}\mathbf{u} + \boldsymbol{\nabla}\mathbf{u}^T\|^2, \tag{21}$$

while $\mathcal{P}_{k\theta}$ is the source term for the temperature fluctuations

$$\mathcal{P}_{k\theta} := -\overline{\mathbf{u}'T'}\cdot\boldsymbol{\nabla}T = \alpha_t\,\|\boldsymbol{\nabla}T\|^2. \tag{22}$$

Preprints (www.preprints.org) | NOT PEER-REVIEWED | Posted: 31 May 2020 doi:10.20944/preprints202005.0503.v1

Peer-reviewed version available at Appl. Sci. 2020, 10, 4337; doi:10.3390/app10124337

The model constants for the KLW model are reported in Table 1, while f_ε and C_{d2} are two functions needed to correct the behavior of the turbulence model near the wall [15,23,24]

$$f_\varepsilon = \left(1 - e^{-0.3226\,R_\delta}\right)^2 \left(1 - 0.3e^{-0.0237\,R_t^2}\right), \tag{23}$$

$$C_{d2} = \left[1.9\left(1 - 0.3\,e^{-0.0237\,R_t^2}\right) - 1\right]\left(1 - e^{-0.0308\,R_\delta}\right)^2. \tag{24}$$

The parameters R_t and R_d are defined in section 2.2.

$C_{1\varepsilon}$	$C_{2\varepsilon}$	C_μ	σ_k	σ_ε	c_{p1}	c_{p2}	c_{d1}	σ_θ
1.5	1.9	0.09	1.4	1.4	1.025	1.9	1.1	1.4

Table 1. Values of the model constants for (17) - (20).

2.2. Model for eddy viscosity and eddy heat diffusivity

The eddy viscosity ν_t and the eddy heat diffusivity α_t are modeled using the turbulent kinetic energy k and two local characteristic time scales τ_{lu} and $\tau_{l\theta}$, the first for the dynamical turbulence and the latter for the thermal turbulence

$$\nu_t = C_\mu k \tau_{lu}, \qquad \alpha_t = C_\theta k \tau_{l\theta}. \tag{25}$$

In order to model the characteristic time scales we use the turbulent Reynolds number R_t and the nondimensional length R_d, as suggested in [15,23,24]. These two quantities are defined using the variables k and ε, in particular

$$R_t := \frac{k^2}{\nu\varepsilon}, \qquad R_d := \frac{\delta}{(\nu^3/\varepsilon)^{1/4}}, \tag{26}$$

where δ is the wall distance and $(\nu^3/\varepsilon)^{1/4}$ is the Kolmogorov length scale [15]. Using the logarithmic variables, R_t and R_d are calculated as

$$R_t = \frac{k}{\nu C_\mu e^\Omega}, \tag{27}$$

$$R_d = \frac{\delta}{\nu}\sqrt{\frac{k}{\sqrt{R_t}}}. \tag{28}$$

We also define a characteristic dynamical time scale $\tau_u = k/\varepsilon = 1/C_\mu e^\Omega$ and a characteristic thermal one $\tau_\theta = k_\theta/\varepsilon_\theta = 1/C_\mu e^{\Omega_\theta}$.

The local characteristic dynamical time scale τ_{lu} is modeled as sum of different contributions [8,15,23,25]

$$\tau_{lu} = \left(f_{1\mu}A_{1\mu} + f_{2\mu}A_{2\mu}\right), \tag{29}$$

where

$$f_{1\mu} = (1 - e^{-R_d/14})^2, \tag{30}$$

$$A_{1\mu} = \tau_u, \tag{31}$$

$$f_{2\mu} = f_{1\mu}e^{-2.5\times10^{-5}R_t^2}, \tag{32}$$

$$A_{2\mu} = \tau_u \frac{5}{R_t^{3/4}}. \tag{33}$$

Preprints (www.preprints.org) | NOT PEER-REVIEWED | Posted: 31 May 2020 doi:10.20944/preprints202005.0503.v1

Peer-reviewed version available at Appl. Sci. 2020, 10, 4337; doi:10.3390/app10124337

The term $A_{1\mu}$ is the bulk dynamical time scale while $A_{2\mu}$ is the correction term for the near wall behavior. The function $f_{2\mu}$ decreases rapidly as the wall distance increases, so the term $f_{2\mu}A_{2\mu}$ is significant only in the near wall region. With this modeling we can correctly reproduce the near wall behavior of the eddy viscosity $\nu_t \propto \delta^3$.

A useful term employed in the modeling of the local thermal characteristic time scale is the thermal to dynamical time scale ratio $R = \tau_\theta/\tau_u = k_\theta\varepsilon/(k\varepsilon_\theta) = e^{\Omega-\Omega_\theta}$. The time scale $\tau_{l\theta}$ is modeled as [8,15,17,18,23,25]

$$\tau_{l\theta} = (f_{1\theta}B_{1\theta} + f_{2\theta}B_{2\theta}) \,, \tag{34}$$

where

$$f_{1\theta} = \left(1 - e^{\sqrt{Pr}R_d/19}\right)\left(1 - e^{R_d/14}\right) \,, \tag{35}$$

$$B_{1\theta} = \frac{\tau_u}{Pr_{t,\infty}} \,, \tag{36}$$

$$f_{2\theta}B_{2\theta} = \tau_u\left(f_{2a\theta}\frac{2R}{C_\gamma + R} + f_{2b\theta}\sqrt{\frac{2R}{Pr}}\frac{1.3}{\sqrt{Pr}R_t^{3/4}}\right) \,, \tag{37}$$

with

$$f_{2a\theta} = f_{1\theta}e^{-(R_t/500)^2} \,, \tag{38}$$

$$f_{2b\theta} = f_{1\theta}e^{-(R_t/200)^2} \,. \tag{39}$$

The time scale $\tau_{l\theta}$ is calculated as the sum of two terms: the first, $B_{1\theta}$, is a bulk term that is a function only of the dynamical time scale τ_u. This term is the most important in the region far from the wall. The second term, $B_{2\theta}$, is the sum of two contributions: a near wall term that is proportional to the time scale $\tau_u\sqrt{R} = \sqrt{\tau_u\tau_\theta}$ and a term that is proportional to the mixed time scale $\tau_m = \tau_u R/(C_\gamma + R)$. This last time scale is calculated as the harmonic mean between the time scales τ_u and τ_θ. With this formulation the model is able to reproduce the near wall behavior of the eddy thermal diffusivity, which is $\alpha_t \propto \delta^3$, when no thermal fluctuations are assumed on the wall surface, and $\alpha_t \propto \delta^2$, when thermal fluctuations are present on the wall surface [8,15,23,25].

We report also Kays model which has been suggested for RANS simulations of liquid metal flows [5,13]. This model can be used to compute the eddy heat diffusivity α_t while the eddy viscosity ν_t needs to be defined in the turbulence model. We consider ν_t as in (25) with the appropriate time scales and model functions already defined. α_t is computed through the definition of a variable turbulent Prandtl number,

$$Pr_t = 0.85 + \frac{0.7}{\frac{\nu_t}{\nu}} \qquad \alpha_t = \frac{\nu_t}{Pr_t} \,, \tag{40}$$

where ν_t/ν is the eddy viscosity ratio. This model has some advantages because it is very simple and not computational expensive and it allows to compute the Pr_t as a local function.

In the Numerical Results Section we compare the results obtained with these two models with DNS data and an experimental correlation for liquid metal flows.

Preprints (www.preprints.org) | NOT PEER-REVIEWED | Posted: 31 May 2020 doi:10.20944/preprints202005.0503.v1

Peer-reviewed version available at Appl. Sci. 2020, 10, 4337; doi:10.3390/app10124337

2.3. Boundary conditions for the turbulence models

Mean components	Fluctuating components
$u = A_1 y + A_2 y^2 + A_3 y^3$	$u' = a_1 y + a_2 y^2 + a_3 y^3$
$v = \quad + B_2 y^2 + B_3 y^3$	$v' = \quad + b_2 y^2 + b_3 y^3$
$w = C_1 y + C_2 y^2 + C_3 y^3$	$w' = c_1 y + c_2 y^2 + c_3 y^3$
$T = D_0 + D_1 y + D_2 y^2$	$T' = d_0 + d_1 y + d_2 y^2$

Table 2. Near wall Taylor series expansion for the components of the mean velocity $\mathbf{u}$, of the fluctuating velocity $\mathbf{u}'$, of the mean temperature T and of the fluctuating temperature T' in a plane channel case where x-z are the axial coordinates and y is the distance from the wall.

In this section we describe the boundary conditions that can be imposed on the variables of the KLW model. When a near-wall approach with no wall function is preferred, the boundary conditions that must be set on wall boundaries can be obtained using a near wall Taylor series expansion for the turbulence variables. For the description of the boundary conditions we refer to the case of a plane channel where x-z are the axial coordinates and y is the wall distance.

We follow the definitions (14-15) and calculate the near wall behaviors of k, ε, k_θ and ε_θ, which are denoted by the lower-script w. Then we combine these behaviors in order to derive the ones of Ω and Ω_θ. In Table 2 the near wall Taylor series expansions are reported for the mean and fluctuating velocity components and for the mean and fluctuating temperature.

For the dynamical turbulence variables we obtain

$$k_w \simeq \frac{1}{2}(a_1^2 + c_1^2) y^2 = \frac{1}{2}\xi y^2 \,, \tag{41}$$

$$\varepsilon_w \simeq \nu(a_1^2 + c_1^2) = \nu\xi \,, \tag{42}$$

$$\Omega_w \simeq \ln\left(\frac{2\nu}{C_\mu y^2}\right) . \tag{43}$$

As we can see from (41) the turbulent kinetic energy tends to zero as the square of the wall distance. By taking the derivative of k in the wall normal direction y we obtain

$$\left.\frac{\partial k}{\partial y}\right|_w = \xi y = \frac{2k_w}{y} \,, \tag{44}$$

so for this variable we can impose the Neumann boundary condition (44). We see that the dissipation of turbulent kinetic energy, ε, in the near wall region does not depend on the wall distance. The near wall behavior is $\varepsilon_w = \nu\xi$, where ξ is a constant value which depends on the fluctuating velocity components. This value cannot be determined *a priori* and it should be calculated as $\xi = 2k_w/y^2$. On wall surfaces we thus impose a Dirichlet b.c. $\varepsilon_w = \nu\xi$ with ξ varying iteration by iteration. This could be a reason of KE model showing poor numerical stability. The KLW model is not affected by this issue because Ω_w depends only on the known kinematic viscosity ν, wall distance y and model constant C_μ, so that it is possible to impose an exact Dirichlet b.c.. If we take the Ω derivative in the wall normal direction we obtain

$$\left.\frac{\partial \Omega}{\partial y}\right|_w = -\frac{2}{y} \,, \tag{45}$$

so we can also impose a Neumann b.c. on wall surfaces. The boundary conditions for the dynamical turbulent variables of the KLW model are summarized in Table 3.

Preprints (www.preprints.org) | NOT PEER-REVIEWED | Posted: 31 May 2020 doi:10.20944/preprints202005.0503.v1

Peer-reviewed version available at Appl. Sci. 2020, 10, 4337; doi:10.3390/app10124337

	Boundary condition			Boundary condition	
Variable	Dirichlet	Neumann	Variable	Dirichlet	Neumann
k_w	-	$\frac{\partial k_w}{\partial y} = \frac{2k_w}{y}$	$k_{\theta w}$	-	$\frac{\partial k_{\theta w}}{\partial y} = \frac{2k_{\theta w}}{y}$
Ω_w	$\Omega_w = \ln\left(\frac{2\nu}{C_\mu y^2}\right)$	$\frac{\partial \Omega_w}{\partial y} = -\frac{2}{y}$	$\Omega_{\theta w}$	$\Omega_{\theta w} = \ln\left(\frac{2\alpha}{C_\mu y^2}\right)$	$\frac{\partial \Omega_{\theta w}}{\partial y} = -\frac{2}{y}$

Table 3. Boundary conditions that can be set on the variables of the KLW model, where the MX b.c. are considered for the thermal variables.

The boundary conditions to be imposed for the thermal turbulent variables are under broad discussion, [8,9,15,23,25]. As it concerns the energy equation, in this paper we apply only boundary conditions of uniform heat flux on the wall surfaces. This kind of b.c. has to be satisfied by both instantaneous and averaged temperature, so the derivative of the fluctuating temperature in the wall normal direction has to be null. In this paper we use the Mixed boundary condition (MX) in which the temperature fluctuation and its derivative on the wall, so the terms d_0 and d_1 in the near wall expansion in Table 2, are set to zero.

With these assumptions on the fluctuating temperature field we obtain the following near wall behaviors

$$k_{\theta w} \simeq \frac{d_2^2}{2} y^2 \,, \tag{46}$$

$$\varepsilon_{\theta w} \simeq \alpha d_2^2 \,, \tag{47}$$

$$\Omega_{\theta w} \simeq \ln\left(\frac{2\alpha}{C_\mu y^2}\right) . \tag{48}$$

We observe that, as for the case of dynamical turbulence, the mean squared temperature fluctuations k_θ is proportional to the squared wall distance while its dissipation $\varepsilon_{\theta w}$ has a constant value. The variable $\varepsilon_{\theta w}$ is thus affected by the same issue of ε_w, so we can only apply a Dirichlet b.c. with a value αd_2^2 that varies iteration by iteration. For the variable $k_{\theta w}$ we impose a Neumann b.c.

$$\frac{\partial k_{\theta w}}{\partial y} = d_2^2 y = \frac{2k_{\theta w}}{y} \,, \tag{49}$$

while for $\Omega_{\theta w}$ we can impose either an exact Dirichlet b.c. or a Neumann b.c., in a similar way as explained for the dynamical turbulence. The boundary conditions that can be imposed on the thermal turbulence variables of the KLW model are reported in Table 3.

We finally observe that if we impose the exact Dirichlet b.c. on the variables Ω and Ω_θ then the thermal to dynamical characteristic time scale ratio R is

$$R = e^{\Omega - \Omega_\theta} = e^{\ln(\nu/\alpha)} = Pr \,. \tag{50}$$

The value of R is equal to Pr on the wall surface, condition that is observed also in DNS simulations with MX b.c. [9].

Preprints (www.preprints.org) | NOT PEER-REVIEWED | Posted: 31 May 2020 doi:10.20944/preprints202005.0503.v1

Peer-reviewed version available at Appl. Sci. 2020, 10, 4337; doi:10.3390/app10124337

3. Numerical results

Property	Symbol		Value	Unit
Viscosity	μ		0.00184	Pa s
Density	ρ		10340	Kg/m^3
Thermal conductivity	λ	$Pr = 0.01$ $Pr = 0.025$	26.818 10.76896	W/(m K)
Heat specific capacity	C_p		146	J/(Kg K)

Table 4. Physical parameters used in the CFD simulations.

In this section we show the results obtained from the simulations performed with the KLW model and with Kays model. We investigate fully developed turbulent flows in plane channels and cylindrical ducts for several values of the Reynolds number. In particular the simulations reported are obtained for a fluid with $Pr = 0.01$ in the plane channel and for fluids with $Pr = 0.01$ and $Pr = 0.025$ in the cylindrical pipes. By reporting these results we aim at extending the validation of our turbulence model to fluids with different Prandtl number. In Table 4 we report the values of the physical properties employed for the simulations.

We implement and solve the system (17-20) together with the Navier-Stokes equations (8-9-13) in an in-house parallel finite element code. We employ Taylor-Hood finite elements for the system of Navier-Stokes in order to satisfy the inf-sup condition and this system is solved with a standard projection method. The two systems of turbulence equations are solved with standard quadratic finite elements.

3.1. Plane channel

The plane channel is one of the most simple geometries and one of the most studied with Direct Numerical Simulations for fully developed turbulent flows of low Prandtl number fluids [9,10]. We report three simulation results of fully developed turbulent flows, in particular for the cases of $Re_\tau = 180$ (A), $Re_\tau = 395$ (B) and $Re_\tau 590$ (C). The corresponding bulk Reynolds number for these cases are respectively $Re = 5760$, 14160 and 22170. DNS data are available for both the dynamical and thermal turbulence for a fluid with $Pr = 0.01$ for the studied cases [10]. We compare the DNS data and the results obtained with the KLW model. The physical domain consists of two plates located at a mutual distance $L = 0.0605$ m. On the wall surfaces a uniform heat flux q per unit area is applied, in particular $q = 3.6 \times 10^5$ W/m^2. We simulate only half of the physical domain because the fully developed turbulent flows presents a symmetry with respect to the middle channel axis. The boundary conditions we apply are reported in Tab. 5. We denote with x the direction normal to the

Var.	Γ_{sym}	$\Gamma_{in} \cup \Gamma_{out}$	Γ_w
u	$u = 0$	$\frac{\partial u}{\partial y} = 0$	$u = 0$
v	$\frac{\partial v}{\partial x} = 0$	$\frac{\partial v}{\partial y} = 0$	$\frac{\partial v}{\partial x} = \frac{\mu}{\delta}$
k	$\frac{\partial k}{\partial x} = 0$	$\frac{\partial k}{\partial y} = 0$	$\frac{\partial k}{\partial x} = \frac{2k}{\delta}$
Ω	$\frac{\partial \Omega}{\partial x} = 0$	$\frac{\partial \Omega}{\partial y} = 0$	$\Omega = \ln\left(\frac{2\nu}{C_\mu \delta^2}\right)$
$\tilde{T}$	$\frac{\partial \tilde{T}}{\partial x} = 0$	$\frac{\partial \tilde{T}}{\partial y} = 0$	$\tilde{T} = 0$
k_θ	$\frac{\partial k_\theta}{\partial x} = 0$	$\frac{\partial k_\theta}{\partial y} = 0$	$\frac{\partial k_\theta}{\partial x} = \frac{2k_\theta}{\delta}$
Ω_θ	$\frac{\partial \Omega_\theta}{\partial x} = 0$	$\frac{\partial \Omega_\theta}{\partial y} = 0$	$\Omega_\theta = \ln\left(\frac{2\alpha}{C_\mu \delta^2}\right)$

Table 5. Boundary conditions imposed for the simulations of fully developed turbulent flows in plane channel.

Preprints (www.preprints.org) | NOT PEER-REVIEWED | Posted: 31 May 2020 doi:10.20944/preprints202005.0503.v1

Peer-reviewed version available at Appl. Sci. 2020, 10, 4337; doi:10.3390/app10124337

wall surfaces and with y the axial direction. The inlet and outlet surfaces are represented with Γ_{in} and Γ_{out} respectively, while Γ_{sym} indicates the symmetry plane and Γ_w the wall surface. The results are nondimensionalized using the kinematic viscosity ν of the fluid, the friction velocity $v_\tau = \sqrt{\tau_w/\rho}$, with τ_w the wall shear stress and ρ the fluid density, and the friction temperature $T_\tau = q/(v_\tau \rho C_p)$, where C_p is the fluid specific heat capacity.

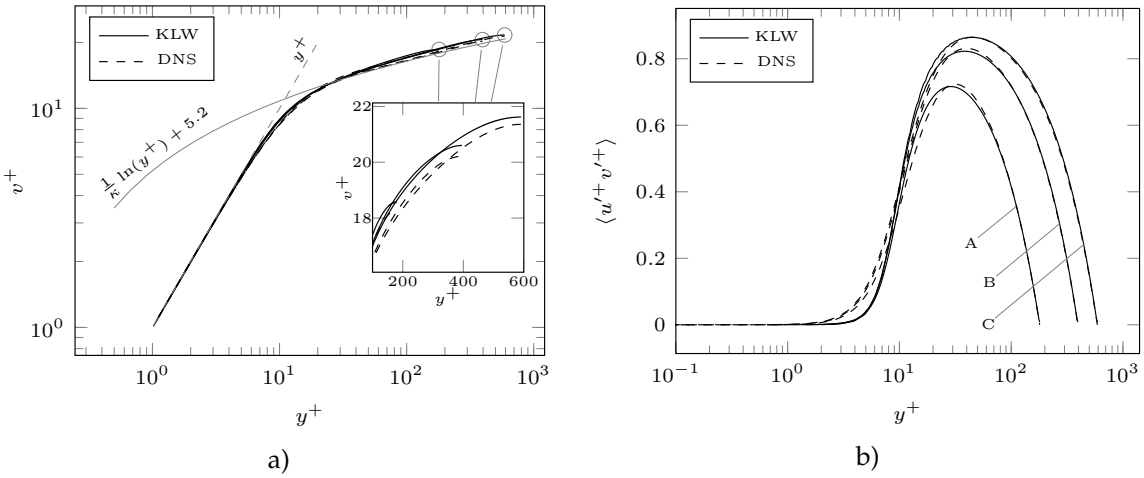

Figure 1. Plane channel, $Pr = 0.01$. Non dimensional mean axial velocity v^+ profiles a) as a function of the nondimensional distance from the wall y^+ and nondimensional Reynolds stresses b) plotted against the nondimensional wall distance y^+. Results obtained with KLW model are compared with DNS data [10].

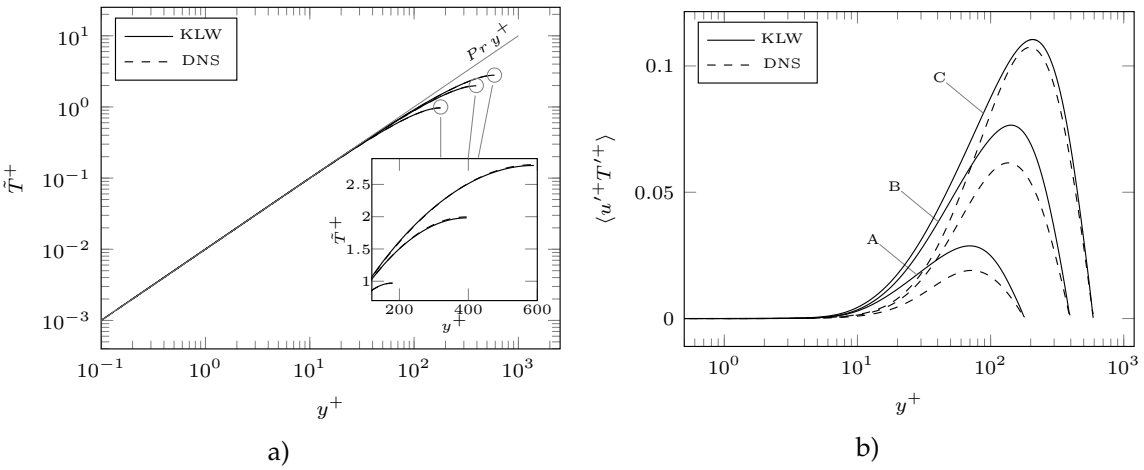

Figure 2. Plane channel, $Pr = 0.01$. Non dimensional mean temperature $\tilde{T}^+$ profiles a) as a function of the nondimensional distance from the wall y^+ and nondimensional turbulent heat flux b) plotted against the nondimensional wall distance y^+. The results obtained with KLW model are compared with DNS data [10].

In Fig. 1 the nondimensional axial velocity profiles v^+ are reported together with the DNS results. We see that the linear behavior $v^+ = y^+$ is well reproduced in the viscous region, while the typical logarithmic behavior $v^+ = 1/\kappa \ln(y^+) + 5.2$ is not reproduced for these small values of the Reynolds number. The comparison with the DNS data shows an overall good agreement between the results. The nondimensional Reynolds stresses $\tau_{uv}^{R+} = \langle u'^+ v'^+ \rangle$ are plotted against the nondimensional wall distance y^+ in Fig. 1 b) and compared with the DNS data. The comparison is good in the logarithmic region ($y^+ > 30$), while some discrepancies are present in the buffer region ($5 < y^+ < 30$) and in a part of the viscous region.

Preprints (www.preprints.org) | NOT PEER-REVIEWED | Posted: 31 May 2020 doi:10.20944/preprints202005.0503.v1

Peer-reviewed version available at Appl. Sci. 2020, 10, 4337; doi:10.3390/app10124337

The nondimensional mean temperature profiles $\tilde{T}^+$ are shown in Fig. 2 a). We see that the linear behavior $\tilde{T}^+ = Pr\, y^+$ is perfectly reproduced and the comparison with the relative DNS data is excellent.

In Fig. 2 b) we report the profiles of the nondimensional turbulent heat flux $\mathbf{q}^{R+} \cdot \hat{n} = \langle u'^+ T'^+ \rangle$ where $\hat{n}$ is the unit vector normal to the wall surface. We see that the agreement with the DNS data is good in the viscous region, while for the remaining part of the domain the agreement with the DNS data is better for the case of $Re_\tau = 590$. However this difference in the turbulent heat flux does not affect the temperature profile because the molecular heat flux has a great importance for this very low Prandtl and Reynolds number also for very high y^+, see [5].

3.2. Cylindrical pipe

In this section we analyze the results we obtained from the simulations of fully developed turbulent flows in a cylindrical pipe. The physical domain consists of a cylinder with a diameter $D = 0.0605$ m. On the wall surface a uniform heat flux q per unit area is applied with value of 3.6×10^5 W/m^2. As for the case of plane channel, we denote with Γ_w the wall surface, with Γ_{in} and Γ_{out} the inlet and outlet sections and with Γ_{sym} the cylinder axis which is the axial symmetry axis of the problem. The boundary conditions we set are reported in Table 6, where r is the radial coordinate, u the radial component of the mean velocity field and v the axial one.

Var.	Γ_{sym}	$\Gamma_{in} \cup \Gamma_{out}$	Γ_w
u	$u = 0$	$\frac{\partial u}{\partial y} = 0$	$u = 0$
v	$\frac{\partial v}{\partial r} = 0$	$\frac{\partial v}{\partial y} = 0$	$\frac{\partial v}{\partial r} = \frac{\mu}{\delta}$
k	$\frac{\partial k}{\partial r} = 0$	$\frac{\partial k}{\partial y} = 0$	$\frac{\partial k}{\partial r} = \frac{2k}{\delta}$
Ω	$\frac{\partial \Omega}{\partial r} = 0$	$\frac{\partial \Omega}{\partial y} = 0$	$\Omega = \ln\left(\frac{2\nu}{C_\mu \delta^2}\right)$
$\tilde{T}$	$\frac{\partial \tilde{T}}{\partial r} = 0$	$\frac{\partial \tilde{T}}{\partial y} = 0$	$\tilde{T} = 0$
k_θ	$\frac{\partial k_\theta}{\partial r} = 0$	$\frac{\partial k_\theta}{\partial y} = 0$	$\frac{\partial k_\theta}{\partial r} = \frac{2k_\theta}{\delta}$
Ω_θ	$\frac{\partial \Omega_\theta}{\partial r} = 0$	$\frac{\partial \Omega_\theta}{\partial y} = 0$	$\Omega_\theta = \ln\left(\frac{2\alpha}{C_\mu \delta^2}\right)$

Table 6. Boundary conditions imposed for the simulations of fully developed turbulent flows in the cylindrical duct geometry.

Case	A	B	C	D	E	F	G
Re_τ	180	360	550	1000	3580	5840	6860
Re	5760	12770	20700	41000	165000	286000	341000

Table 7. Fully developed turbulent flows simulated cases for the cylindrical geometry.

The simulated cases of fully developed turbulent flows with both $Pr = 0.01$ and $Pr = 0.025$ are reported in Table 7 together with the relative value of the turbulent Reynolds number Re_τ and of the Reynolds number Re. The physical properties of such fluids are reported in Table 4. We compare the different thermal results of the two fluids and see how the turbulent variables are influenced by the different Prandtl number. Finally we compute the Nusselt number values of every simulation and compare them with the experimental correlations in order to demonstrate that the turbulence model gives reliable results for different Prandtl numbers. In this geometry we study also the Kays model. The same test cases are carried out for this model and the same comparison with the experimental correlations is given.

Preprints (www.preprints.org) | NOT PEER-REVIEWED | Posted: 31 May 2020 doi:10.20944/preprints202005.0503.v1

Peer-reviewed version available at Appl. Sci. 2020, 10, 4337; doi:10.3390/app10124337

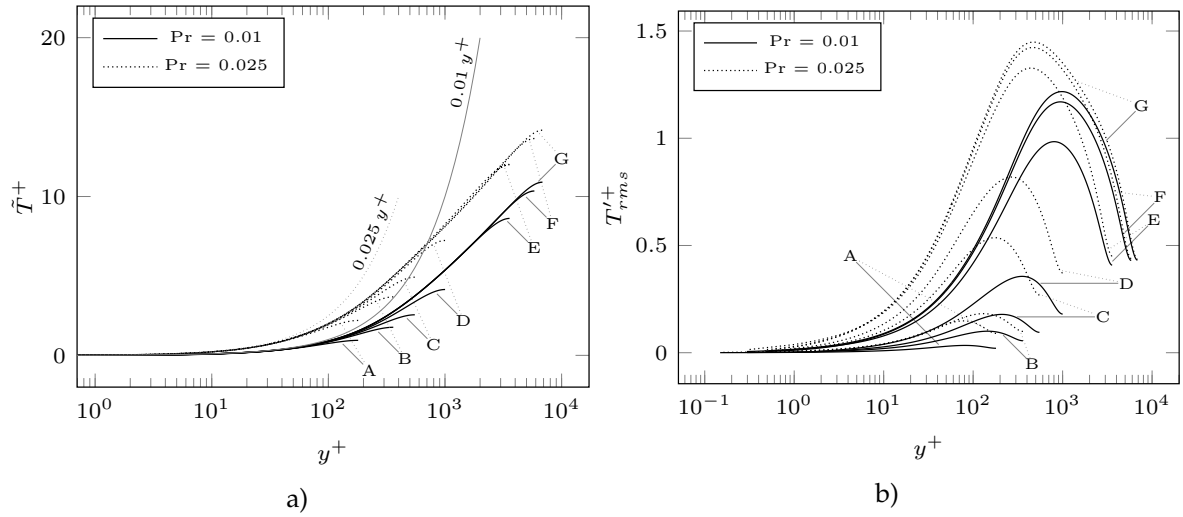

Figure 3. Cylindrical pipe. Non dimensional profiles of the mean temperature $\tilde{T}^+$ a) and of the root mean squared temperature fluctuations T'^+_{rms} b) for the simulations of $Pr = 0.025$ and $Pr = 0.01$ with the KLW model.

Re_τ	$Pr = 0.01$			$Pr = 0.025$		
	$\tilde{T}^+_m$	$T'^+_{rms,m}$	$T'^+_{rms,m}/\tilde{T}^+_m$	$\tilde{T}^+_m$	$T'^+_{rms,m}$	$T'^+_{rms,m}/\tilde{T}^+_m$
180	0.62	0.025	0.041	1.46	0.112	0.076
360	1.17	0.075	0.064	2.53	0.275	0.108
550	1.71	0.134	0.078	3.44	0.402	0.117
1000	2.82	0.268	0.095	5.16	0.609	0.117
3578	6.35	0.711	0.111	9.30	0.895	0.096
5843	7.85	0.814	0.103	10.82	0.896	0.082
6852	8.34	0.836	0.100	11.32	0.918	0.081

Table 8. Cylindrical pipe. Mean values across the transverse section of the pipe: RMS temperature fluctuations $T'^+_{rms,m}$, mean temperature $\tilde{T}^+_m$ and the ratio $T'^+_{rms,m}/\tilde{T}^+_m$.

In Fig. 3 a) the nondimensional temperature $\tilde{T}^+$ profiles are reported for the simulated cases. We see that the linear behavior $\tilde{T}^+ = Pr\, y^+$ is well reproduced. In Fig. 3 b) the nondimensional root mean squared temperature fluctuation k_θ is plotted against the nondimensional wall distance y^+ for all the simulated cases and for both $Pr = 0.01$ and $Pr = 0.025$. We can see how the different molecular Prandtl number affects the temperature fluctuations. In particular we see that the simulations with $Pr = 0.01$ are characterized by a maximum value of T'^+_{rms} which is smaller than the one obtained with $Pr = 0.025$ and the peak position is shifted nearer the pipe middle axis. In Table 8 we report the mean values across the pipe transverse section of nondimensional mean temperature and nondimensional RMS temperature fluctuations

$$\tilde{T}^+_m = \frac{2}{D}\int_0^{D/2} \tilde{T}^+ dr \qquad T'^+_{rms,m} = \frac{2}{D}\int_0^{D/2} T'^+_{rms} dr\,, \tag{51}$$

together with their ratio $T'^+_{rms,m}/\tilde{T}^+_m$. These parameters allow to compare the mean temperature fluctuations modulus with the mean difference between the fluid temperature and the solid wall one. For low velocities with $Re_\tau \leq 1000$ we see that the temperature fluctuations increase for increasing mean velocities and are higher for $Pr = 0.025$ than for $Pr = 0.01$. For the cases $Re_\tau > 1000$ we observe that the importance of the temperature fluctuations, relative to the mean temperature, decreases for increasing velocities and that it is higher for $Pr = 0.01$ than for $Pr = 0.025$.

Preprints (www.preprints.org) | NOT PEER-REVIEWED | Posted: 31 May 2020 doi:10.20944/preprints202005.0503.v1

Peer-reviewed version available at Appl. Sci. 2020, 10, 4337; doi:10.3390/app10124337

The heat transfer between a wall surface and a fluid flow is usually evaluated through the calculation of the Nusselt number. This is a nondimensional parameter that takes into account the thermal conductivity λ of the fluid, the hydraulic diameter D_h of the transverse section of the pipe and the convective heat transfer coefficient h. The Nusselt number is then calculated as

$$Nu = \frac{hD_h}{\lambda}\,. \tag{52}$$

For the case of a constant heat flux per unit surface q applied on wall surfaces, the convective heat transfer coefficient can be expressed as

$$h = \frac{q}{T_w - T_b}\,, \tag{53}$$

where T_w is the wall surface temperature and T_b is a representative temperature of the fluid. Normally T_b is the bulk temperature of the fluid

$$T_b = \frac{\int_A T\mathbf{u}\cdot\hat{n}dA}{\int_A \mathbf{u}\cdot\hat{n}dA}\,, \tag{54}$$

where $\hat{n}$ is the unit vector normal to the transverse section A of the pipe.

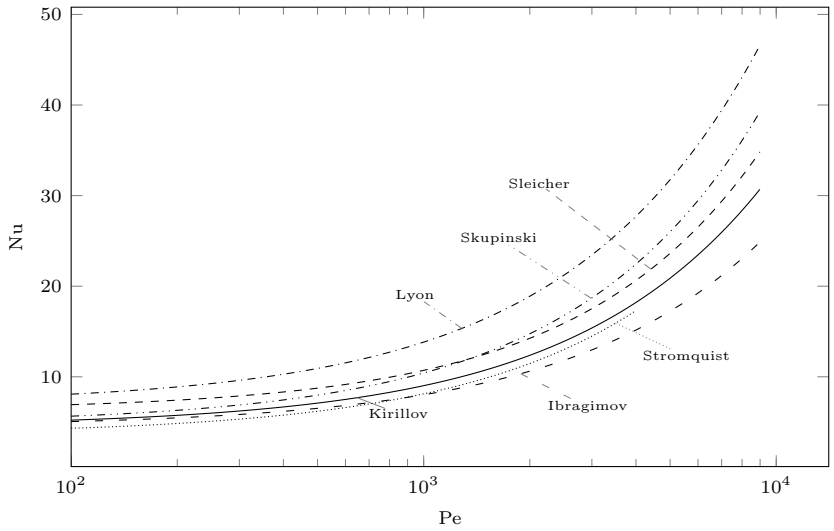

Figure 4. Cylindrical pipe heated with constant heat flux. Representation of the Nusselt number experimental correlations (56)–(61) as a function of the Peclet number.

In literature many correlations based on experimental results of liquid metal flows in cylindrical geometry for the calculation of the Nusselt number are available. The general form of these correlations is

$$Nu = A + a\,Pe^n\,, \tag{55}$$

Preprints (www.preprints.org) | NOT PEER-REVIEWED | Posted: 31 May 2020 doi:10.20944/preprints202005.0503.v1

Peer-reviewed version available at Appl. Sci. 2020, 10, 4337; doi:10.3390/app10124337

where Pe is the Peclet number and A, a and n are constant positive numbers. We report some of the main correlations for the case of cylindrical pipe heated with constant heat flux with their range of validity expressed in terms of Reynolds number value or Peclet value.

$$Nu = 7.0 + 0.025 \left(\frac{Pe}{Pr_t} \right)^{0.8} \qquad 10^4 \leq Re \leq 5 \cdot 10^6 , \tag{56}$$

$$Nu = 4.82 + 0.0185 Pe^{0.827} \qquad 10^4 \leq Re \leq 5 \cdot 10^6 , \tag{57}$$

$$Nu = 6.3 + 0.0167 Pe^{0.85} Pr^{0.08} \qquad 10^4 \leq Re \leq 5 \cdot 10^6 , \tag{58}$$

$$Nu = 4.5 + 0.014 Pe^{0.8} \qquad 10^4 \leq Re \leq 5 \cdot 10^6 , \tag{59}$$

$$Nu = 3.6 + 0.018 Pe^{0.8} \qquad 88 \leq Pe \leq 4000 . \tag{60}$$

$$Nu = 4.5 + 0.018 Pe^{0.8} \qquad 10^4 < Re < 5 \cdot 10^6 . \tag{61}$$

All these correlations (56)–(61) are plotted in Fig. 4. The correlation proposed by Lyon (56) is one of the first correlations for liquid metals and uses the turbulent Prandtl number Pr_t [26,27]. In Fig. 4 the Lyon's correlation is plotted with $Pr_t = 0.9$. As we can see the correlation gives values of the Nusselt number which are much greater than the ones of the other correlations. The Skupinski and Sleicher correlations (57, 58) were obtained using experimental heat transfer data of NaK [28,29]. Ibragimov derived (59) using experimental data of LBE heat transfer while (60) is based on values of heat transfer obtained using mercury by Stromquist [30,31]. Recently Kirillov proposed a new correlation based on a long analysis on existing correlations and experimental data as (61) [32].

As it can be seen from Figure 4 there is an overall disagreement between the different correlations that have been proposed for the Nusselt number. An explanation for these discrepancies is given in [4]. By a comparison with the only freely available experimental data present in literature [4,33] it is shown that the Kirillov correlation is the one that fits better the experimental points in the low Peclet region ($Pe < 1000$), while in the high Peclet region ($Pe > 2000$) the Stromquist correlation shows a better agreement with the experimental values. For this reason the authors in [4] proposed a new correlation based on a fit of these two correlations in the range of their best approximation,

$$\begin{aligned} Nu &= A + 0.018 Pe^{0.8} , \\ A &= \begin{cases} 4.5 & Pe < 1000 , \\ 5.4 - 9 \times 10^{-4} Pe & 1000 \leq Pe \leq 2000 , \\ 3.6 & Pe > 2000 . \end{cases} \end{aligned} \tag{62}$$

This new correlation is equal to the Kirillov one in the low Peclet region and it is equal to the Stromquist in the high Peclet region, with an extension of its validity beyond $Pe = 4000$.

Preprints (www.preprints.org) | NOT PEER-REVIEWED | Posted: 31 May 2020 doi:10.20944/preprints202005.0503.v1

Peer-reviewed version available at Appl. Sci. 2020, 10, 4337; doi:10.3390/app10124337

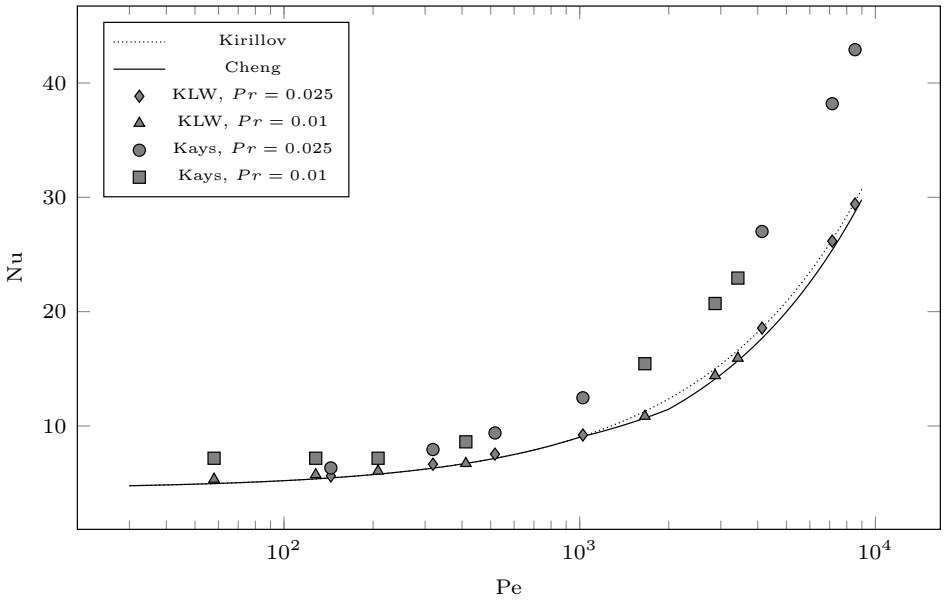

Figure 5. Cylindrical pipe. Nusselt number values for the simulations performed for fluids with $Pr = 0.025$ and $Pr = 0.01$ with KLW and Kays model. The values are compared with the Kirillov correlation and with the Cheng correlation.

Pr	Source	Reynolds number						
		341360	285800	165400	41000	20680	12760	5760
0.025	KLW	29.4092	26.1685	18.5608	9.2123	7.5382	6.6523	5.6329
	Kays	42.9137	38.1888	27.0105	12.4689	9.3894	7.9416	6.3323
	Kirillov	29.6295	26.3008	18.5779	9.1108	7.1690	6.3135	5.4593
	Cheng	28.7295	25.4008	17.6779	9.0885	7.1690	6.3135	5.4593
0.01	KLW	15.9311	14.4070	10.8496	6.7213	6.0596	5.7411	5.3430
	Kays	22.9363	20.7126	15.4458	8.6137	7.1788	6.5008	5.7193
	Kirillov	16.6110	15.0068	11.2848	6.7221	5.7863	5.3740	4.9623
	Cheng	15.7110	14.1068	10.6900	6.7221	5.7863	5.3740	4.9623

Table 9. Nusselt number values obtained with the KLW and Kays model for $Pr = 0.025$ and $Pr = 0.01$ compared with the Kirillov and the Cheng correlation.

In Figure 5 we compare the results obtained with the KLW and with Kays model for the simulations of fully developed turbulent flows of fluids with $Pr = 0.025$ and $Pr = 0.01$ with the Kirillov correlation and the one reported in [4]. For a better interpretation of the obtained results we report in Table 9 the values obtained with the turbulence models together with the values of Kirillov and Cheng correlation. In the Table the values of Nu for $Pr = 0.025$ and $Pr = 0.01$ are compared for the different cases in terms of Reynolds number. As we can see, for the case of $Pr = 0.025$ the values of the KLW model are closer to the Kirillov correlation than to the Cheng correlation as it concerns $Pe > 1000$, while the values obtained for $Pr = 0.01$ are closer to the Cheng correlation. In general we observe that the values obtained with the KLW model lay between the Kirillov and the Cheng correlations, in the high Peclet region, while in the low Peclet region they are slightly greater than the Kirillov correlation. With respect to Kays model we can see that for low Peclet and Prandtl numbers the results are greater than those obtained with KLW model and predicted by both correlations while with increasing Peclet the mismatch becomes very large. This fact can be explained by looking at the definition (40): if the eddy viscosity ratio becomes very high, as it happens for high Peclet numbers, the average turbulent Prandtl number of the channel as computed in (40) approaches 0.85 which is

Preprints (www.preprints.org) | NOT PEER-REVIEWED | Posted: 31 May 2020 doi:10.20944/preprints202005.0503.v1

Peer-reviewed version available at Appl. Sci. 2020, 10, 4337; doi:10.3390/app10124337

known to be not valid for liquid metal flows. Given the differences with the reference data in this very simple geometry the Kays model should be used with care.

4. Conclusions

In this work we have discussed the problem of turbulence modeling to study turbulent heat transfer in liquid metal flows with different low-Prandtl numbers. Two approaches have been compared, Kays model and a logarithmic k-Ω-k_θ-Ω_θ turbulence model, to be used in engineering applications involving the study of fully developed turbulent liquid metal flows. Numerical results in plane and channel geometry have been reported for two different Prandtl numbers, $Pr = 0.01$ and $Pr = 0.025$. The comparison between the numerical results obtained with the four parameter turbulence model with DNS data and experimental correlations can be considered satisfactory for a wide range of Peclet numbers and for both the Prandtl numbers studied. On the other hand the Kays model seems to be not fully appropriate for the study of these flows, especially for high Peclet numbers. The four parameter turbulence model can thus be used as a reliable tool for the study of turbulent flows of liquid metals characterized by low Prandtl numbers between 0.01 and 0.025.

Author Contributions: For research articles with several authors, a short paragraph specifying their individual contributions must be provided. The following statements should be used "Conceptualization, X.X. and Y.Y.; methodology, X.X.; software, X.X.; validation, X.X., Y.Y. and Z.Z.; formal analysis, X.X.; investigation, X.X.; resources, X.X.; data curation, X.X.; writing–original draft preparation, X.X.; writing–review and editing, X.X.; visualization, X.X.; supervision, X.X.; project administration, X.X.; funding acquisition, Y.Y. All authors have read and agreed to the published version of the manuscript.", please turn to the CRediT taxonomy for the term explanation. Authorship must be limited to those who have contributed substantially to the work reported.

Funding: Please add: "This research received no external funding" or "This research was funded by NAME OF FUNDER grant number XXX." and and "The APC was funded by XXX". Check carefully that the details given are accurate and use the standard spelling of funding agency names at https://search.crossref.org/funding, any errors may affect your future funding.

Acknowledgments: In this section you can acknowledge any support given which is not covered by the author contribution or funding sections. This may include administrative and technical support, or donations in kind (e.g., materials used for experiments).

Conflicts of Interest: Declare conflicts of interest or state "The authors declare no conflict of interest." Authors must identify and declare any personal circumstances or interest that may be perceived as inappropriately influencing the representation or interpretation of reported research results. Any role of the funders in the design of the study; in the collection, analyses or interpretation of data; in the writing of the manuscript, or in the decision to publish the results must be declared in this section. If there is no role, please state "The funders had no role in the design of the study; in the collection, analyses, or interpretation of data; in the writing of the manuscript, or in the decision to publish the results".

References

1. Grötzbach, G. Challenges in low-Prandtl number heat transfer simulation and modelling. *Nuclear Engineering and Design* **2013**, *264*, 41–55.
2. Marocco, L.; Cammi, G.; Flesch, J.; Wetzel, T. Numerical analysis of a solar tower receiver tube operated with liquid metals. *International Journal of Thermal Sciences* **2016**, *105*, 22–35.
3. Fazio, C., Ed. *Handbook on Lead-bismuth Eutectic Alloy and Lead Properties, Materials Compatibility, Thermal-hydraulics and Technologies*; OECD, 2015.
4. Cheng, X.; Tak, N.i. Investigation on turbulent heat transfer to lead–bismuth eutectic flows in circular tubes for nuclear applications. *Nuclear Engineering and Design* **2006**, *236*, 385–393.
5. Duponcheel, M.; Bricteux, L.; Manconi, M.; Winckelmans, G.; Bartosiewicz, Y. Assessment of RANS and improved near-wall modeling for forced convection at low Prandtl numbers based on LES up to $Re_\tau = 2000$. *International Journal of Heat and Mass Transfer* **2014**, *75*, 470–482. doi:10.1016/j.ijheatmasstransfer.2014.03.080.
6. Bricteux, L.; Duponcheel, M.; Winckelmans, G.; Tiselj, I.; Bartosiewicz, Y. Direct and large eddy simulation of turbulent heat transfer at very low Prandtl number: Application to lead-bismuth flows. *Nuclear Engineering and Design* **2012**, *246*, 91–97.

Preprints (www.preprints.org) | NOT PEER-REVIEWED | Posted: 31 May 2020 doi:10.20944/preprints202005.0503.v1

Peer-reviewed version available at Appl. Sci. 2020, 10, 4337; doi:10.3390/app10124337

7. Shams, A.; Roelofs, F.; Baglietto, E.; Lardeau, S.; Kenjeres, S. Assessment and calibration of an algebraic turbulent heat flux model for low-Prandtl fluids. *International Journal of Heat and Mass Transfer* **2014**, *79*, 589–601.
8. Manservisi, S.; Menghini, F. A CFD four parameter heat transfer turbulence model for engineering applications in heavy liquid metals. *International Journal of Heat and Mass Transfer* **2014**, *69*, 312–326.
9. Kawamura, H.; Abe, H.; Matsuo, Y. DNS of turbulent heat transfer in channel flow with respect to Reynolds and Prandtl number effects. *International Journal of Heat and Fluid Flow* **1999**, *20*, 196–207.
10. Tiselj, I.; Cizelj, L. DNS of turbulent channel flow with conjugate heat transfer at Prandtl number 0.01. *Nuclear Engineering and Design* **2012**, *253*, 153–160.
11. Hoyas, S.; Jiménez, J. Reynolds number effects on the Reynolds-stress budgets in turbulent channels. *Physics of Fluids* **2008**, *20*.
12. Lozano-Durán, A.; Jiménez, J. Effect of the computational domain on direct simulations of turbulent channels up to $Re_\tau = 4200$. *Physics of Fluids* **2014**, *26*.
13. Kays, W. Turbulent Prandtl number. Where are we? *Journal of Heat Transfer* **1994**, *116*, 284–295.
14. Abe, K.; Suga, K. Towards the development of a Reynolds-averaged algebraic turbulent scalar-flux model. *International Journal of Heat and Fluid Flow* **2001**, *22*, 19–29.
15. Abe, K.; Kondoh, T.; Nagano, Y. A new turbulence model for predicting fluid flow and heat transfer in separating and reattaching flows I. Flow field calculations. *International Journal of Heat and Mass Transfer* **1994**, *37*, 139–151.
16. Hwang, C.; Lin, C. A low Reynolds number two-equation kt-et model to predict thermal field. *International Journal of Heat and Mass Transfer* **1999**, *42*, 3217–3230.
17. Manservisi, S.; Menghini, F. Triangular rod bundle simulations of a CFD k-ε-k_θ-ε_θ heat transfer turbulence model for heavy liquid metals. *Nuclear Engineering and Design* **2014**, *273*, 251–270.
18. Manservisi, S.; Menghini, F. CFD simulations in heavy liquid metal flows for square lattice bare rod bundle geometries with a four parameter heat transfer turbulence model. *Nuclear Engineering and Design* **2015**, *295*, 251–260.
19. Cerroni, D.; Và, R.D.; Manservisi, S.; Menghini, F.; Pozzetti, G.; Scardovelli, R. Numerical validation of a k-ω-k_θ-ω_θ heat transfer turbulence model for heavy liquid metals. *Journal of Physics: Conference Series* **2015**, *655*.
20. Ilinca, F.; Hetu, J.; Pelletier, D. A unified finite element algorithm for two-equation models of turbulence. *Computers & Fluids* **1998**, *27*, 291–310.
21. Wilcox, D.C. *Turbulence Modeling for CFD*, 3 ed.; DCW Industries, Inc., 2006.
22. Hanjalić, K.; Launder, B. *Modelling Turbulence in Engineering and the Environment*; Cambridge University Press, 2011. Cambridge Books Online.
23. Nagano, Y.; Shimada, M. Development of a two equation heat transfer model based on direct simulations of turbulent flows with different Prandtl numbers. *Physics of Fluids* **1996**, *8*, 3379–3402.
24. Abe, K.; Kondoh, T.; Nagano, Y. A new turbulence model for predicting fluid flow and heat transfer in separating and reattaching flows II. Thermal field calculations. *International Journal of Heat and Mass Transfer* **1995**, *38*, 1467–1481.
25. Hattori, H.; Nagano, Y.; Tagawa, M. Analysis of turbulent heat transfer under various thermal conditions with two-equation models. *Engineering Turbulence Modelling and Experiments* **2014**, *2*, 43–52.
26. Lyon, R. Liquid metal heat transfer coefficients. *Chemical Engineering Progress* **1951**, *47*, 75–79.
27. Lyon, R. *Liquid-Metals Handbook*; Atomic Energy Comm., 1952.
28. Skupinski, E.; Tortel, J.; Vautrey, L. Determination des coefficients de convection d'un alliage sodium-potassium dans un tube circulaire. *International Journal of Heat and Mass Transfer* **1965**, *8*, 937–951.
29. Sleicher, C.A.; Awad, A.S.; Notter, R.H. Temperature and eddy diffusivity profiles in NaK. *International Journal of Heat and Mass Transfer* **1973**, *16*, 1565–1575.
30. Ibragimov, M.; Subbotin, V.; Ushakov, P. Investigation of heat transfer in the turbulent flow of liquid metals in tubes. *Atomnaya Energiya* **1960**, *8 (1)*, 54–56.
31. Stromquist, W.K. Effect of wetting on heat transfer characteristics of liquid metals. *ORO-93* **1953**. University of Tennessee.
32. Kirillov, P.; Ushakov, P. Heat transfer to liquid metals: specific features, methods of investigation, and main relationships. *Thermal Engineering* **2001**, *48 (1)*, 50–59.

Preprints (www.preprints.org) | NOT PEER-REVIEWED | Posted: 31 May 2020 doi:10.20944/preprints202005.0503.v1

Peer-reviewed version available at Appl. Sci. 2020, 10, 4337; doi:10.3390/app10124337

33. Johnson, H.; Hartnett, J.; Clabaugh, W. Heat transfer to molten lead–bismuth eutectic in turbulent pipe flow. *Journal of Heat Transfer* **1953**, pp. 1191–1198.